# Photoelectric effects in x-ray preionization for excimer laser gases

A. V. Azarov, P. J. M. Peters,[a] and K.-J. Boller
*Laser Physics and Nonlinear Optics Group, MESA+ Research Institute, Faculty of Science and Technology, University of Twente, P.O. Box 217, 7500 AE Enschede, Netherlands*

(Received 2 August 2007; accepted 10 December 2007; published online 20 February 2008)

We present detailed measurements on the x-ray preionization electron density in a discharge chamber filled with different gases relevant to discharge pumped high-pressure excimer lasers. By comparing experimental results with the theoretical electron densities, we conclude that the observed preionization is inconsistent with the standard picture of direct ionization through x-ray absorption in the gas. We conclude that depending on the gas pressure, type of gas, and the gap length between the discharge electrodes used, x-ray preionization in excimer gases is, to a significant extent or even dominantly, based on a different mechanism. We identify that this mechanism is based on fast photoelectrons emitted by the cathode into the discharge chamber.
 [DOI: 10.1063/1.2841801]

## I. INTRODUCTION

Obtaining powerful radiation with high beam quality from excimer lasers requires that the glow discharge necessary for exciting the laser gas mixture is ignited with high spatial homogeneity.[1,2] A widely accepted approach is to preionize the laser gas with a short pulse of x rays before the pumping discharge is ignited.[3] In order to obtain a homogeneous preionization, the properties of the x-ray source and how its radiation is injected are of central importance. The experimental determination of the initial electron density in x-ray ionized gases has been extensively studied for many years.[4–6] Nevertheless, these issues are usually seen rather simply, namely, that the x rays are absorbed in the gas where they create a sufficiently high and homogeneous electron density. In this view, a homogeneous preionization would be easily achieved providing x rays of suitable photon energy (typically beyond 50 keV), and intensity that traverse a sufficient absorption length in the gas used. In the same view, the transmission of the x rays from the source into the discharge volume, usually through a window in the cathode of the discharge cell, is considered of minor relevance, as long as the window does not attenuate the x rays too much.

Here we show with preionization experiments that this physical picture of x-ray preionization in excimer lasers is incomplete and that the expected preionization electron density achieved by x rays in such systems can be quite different. The consequences of this may affect our understanding of the origin of discharge instabilities in high-pressure excimer laser gas mixtures. Consequently it may influence the search for measures to suppress such instabilities, and can therefore be important for optimizing the design of high quality excimer lasers. For our experiments we use an ionization test chamber filled with various gases and gas mixtures at pressures that are of relevance for high-power excimer lasers. Short x-ray pulses, containing Bremsstrahlung and characteristic radiation, are generated by a corona-discharge-based source in a separate vacuum chamber. The x rays are transmitted into the ionization chamber through a window in the cathode. This arrangement is typical for x-ray preionization in excimer lasers, and its advantage is a well defined volume where the main discharge is to be ignited for laser operation.

We find experimentally that fast photoelectron emission, caused by the absorption of x rays in the surface layer of the cathode, is a significant source of preionization electrons. This mechanism boosts the preionization electron density far beyond that predicted by direct x ray ionization in the gas. Additionally, it was found that the photoelectron contribution was much more significant in light gases. The general presence of such wall-related effects has been known since the original work of Bragg *et al.* who started to quantify the absolute strength of ionizing radiation.[7–10] Nevertheless, such electrode effects have gone unnoticed for x-ray preionization of excimer laser gases. Furthermore, our preionization experiments suggest that these electrode effects have been underestimated.

## II. EXPERIMENTAL SETUP

The X-ray source employed for preionization is based on a pulsed corona discharge[6,11–15] in a grounded vacuum vessel ($10^{-4}$ mbar), as depicted in the lower part of Fig. 1. This x-ray source is very attractive for excimer laser preionization due to its simple and reliable design and its long lifetime (more than $10^8$ shots[12]). Further advantages are the short rise time and duration of the e-beam pulse, typically 10 and 50 ns, respectively,[6,15] which provides a high x-ray peak power. Repetition rates of up to 1 kHz (Refs. 1 and 14) can be achieved, which is of importance for excimer lasers with high average power. In our setup, electrons from the corona discharge are accelerated to an energy of about 100 keV by a homemade six-stage mini-Marx generator, with 17 kV per stage from a high voltage (HV) dc power supply (Hipotronics R 60A). Triggering is achieved with a Farnell PG102 pulse generator, via a homemade triggering unit that switches a thyratron (Perkin Elmer 7665A). The accelerated electrons are directed toward a thin, high-$Z$ foil target, where x rays,

[a]Electronic mail: p.j.m.peters@tnw.utwente.nl.

 

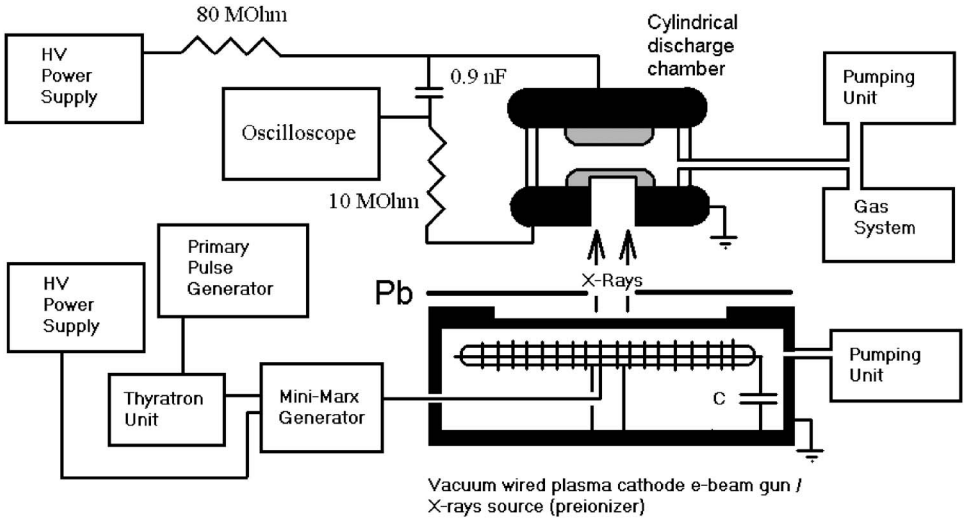


FIG. 1. Experimental setup for measurements of the preionization electron density.

consisting of Bremsstrahlung and characteristic radiation, are produced upon hitting the target. The x-ray radiation leaves the source through a 1 cm diameter aperture in a 2.5 mm thick lead plate.

The preionization measurements in different gases and gas mixtures are performed with a discharge chamber, which is mounted on top of the x-ray source (see upper part in Fig. 1). After evacuation, the chamber is filled with He, Ne, Ar, or with gas mixtures containing a low amount of Xe and $F_2$. A total pressure of up to 5 bars, as is typically employed in excimer lasers, was used. The distance from the x-ray output aperture to the discharge chamber input window is approximately 70 mm. The discharge chamber consists of a cylindrical quartz tube with an inner diameter of 74 mm, enclosed by two Al flanges. Two Al electrodes are attached to the flanges. Both electrodes have rounded edges to prevent high field strengths and are covered with a thin layer of Ni ($\approx 30$ $\mu$m). The lower flange has a round, centered opening of 1 cm in diameter, and the back of the attached cathode possesses a cavity of 1 cm in diameter, to form a 1 mm thick input window for the x-ray pulse.

The upper electrode is 50 mm in diameter and serves as the anode. The lower electrode is 60 mm in diameter, is grounded, and serves as the cathode. The gap length between the electrodes, $d$, is adjustable between 0.5 and 2 cm. The capacitances of the gap, $C_P$, formed by the electrodes and flanges, were measured to be 92 pF (for $d=0.5$ cm), 82 pF ($d=1$ cm), 79 pF ($d=1.5$ cm), and 76 pF ($d=2$ cm).

Prior to the preionization measurements in the discharge chamber, the duration of the x-ray pulse was measured with a scintillator NE102A attached to a photomultiplier tube (Philips 56AVP), placed and centered 10 cm above of the x-ray source output aperture. The full width at half maximum of the x-ray pulse was measured to be $\approx 30$ ns. The x-ray dose inside the discharge chamber was measured to be 1 mrad/pulse by using a pen dosimeter (SEQ6 0.1 rad, 18 keV to 6 MeV). For measurements of the electron density, a dc voltage of up to 4 kV is applied to the anode of the discharge chamber from a HV power supply (Philips 9412) through an 80 M$\Omega$ resistance. Transient discharge currents caused by x-ray induced creation of free charges in the chamber show up as transient changes of the discharge voltage and are monitored with a digital oscilloscope (Tektronix TDS 640A) and a HV probe (Hameg HZ36, division coefficient of 1:10). The probe contains a 0.9 nF capacitor and an effective impedance of 10 M$\Omega$ in series, connecting the discharge electrodes (see Fig. 1).

## III. PREIONIZATION MEASUREMENTS

Preionization measurements in pure gases were performed with He, Ne, and Ar at a gas pressure of 5 bars for electrode gap lengths of $d=0.5$, 1, 1.5, and 2 cm. Additionally the pressure dependence of the preionization on the gas pressure ($p=1$, 2, 3, and 4 bars) was explored for He gas at a gap length of 1.5 cm. Gas mixtures with He and Xe (ratio of 99:1) and He and $F_2$ (99.9:0.1) at 5 bar total pressure were also investigated at an electrode gap length of 1 cm.

In order to collect all the generated electrons a sufficiently high dc voltage, called the saturation voltage, was applied across the electrodes. This voltage should not be too high in order to prevent electron multiplication. We varied the applied dc voltage for every gas or gas mixture and for every gap length used. The choice of the saturation voltage is discussed later in the text.

Figure 2 displays the average of five waveforms received from the (1:10) HV probe as a function of time. The shown traces were recorded with He (1), Ne (2), and Ar (3) at a gas pressure of $p=5$ bars, a gap length of $d=1$ cm, and a voltage of $V_{IC}=1$ kV applied to the electrodes in the ionization chamber. All traces show a negative dip on a millisecond time scale with a typical peak amplitude of the order of $-10$ mV, indicating a transient discharge current caused by x-ray induced generation of free charges in the chamber. Note, however, that the displayed traces in Fig. 2 must be multiplied by a factor of 10, meaning that the discharge voltage dips $\Delta U$ are about 100 mV. The initial short spikes at $t=0$ ms were identified as rf pickup noise and were disregarded. This short spike is present even when the x-ray source is shielded from the discharge chamber by a thick Pb plate. On the other hand, the negative signal decreases when the x-ray source is shielded with an increasing number of

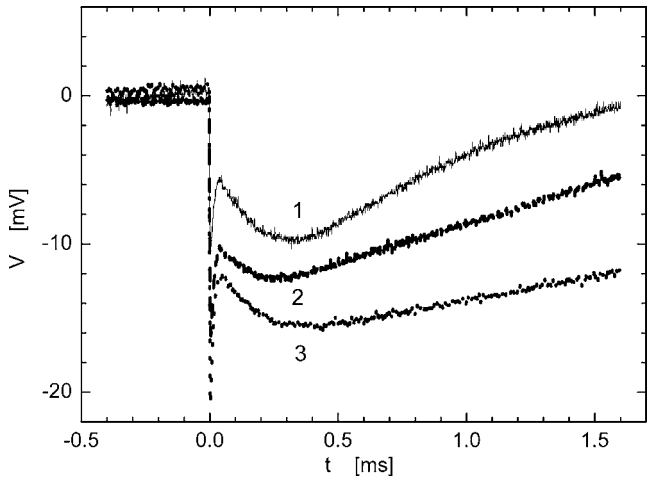


FIG. 2. Preionization signal recorded in He [Eq. (1)], Ne [Eq. (2)], and Ar [Eq. (3)] with $p=5$ bars, $d=1$ cm and $V_{IC}=1$ kV.

13 $\mu$m Al foils. It completely vanishes when a shielding Pb plate is placed between the x-ray source and the discharge chamber. Therefore, this signal is due to gas ionization. Except for a slight shot-to-shot fluctuation in the overall amplitude of the traces, the peak values ($\Delta U$) and time constants found in the voltage traces showed a systematic dependence on the gap length, the applied voltage, the gas pressure, and the type of gas or mixture used.

Figure 2 shows that, in particular, each trace exhibits a specific (negative) peak voltage $\Delta U$ and a final (positive) slope of voltage recovery. For example, in Fig. 3 the traces reach different peak values (at around $t=0.3$ ms), with $|\Delta U|$ being the biggest for Ar (157 mV), smaller for Ne (125 mV), and smallest for He (100 mV). Thereafter, the voltage recovery is the fastest for He, slower for Ne, and slowest for Ar.

In general, it can be expected that the peak voltage and time constants in each trace depend on the number of electron-ion pairs created by x-ray ionization, the electron and ion drift velocities, and the *RC*-time constant of the measurement circuit. Thus, in order to extract absolute values for the ionization electron density, the time scales of the named effects must be compared. In particular, when the mobility of the ions is low compared to that of the electrons, and the *RC* response time of the circuit is long compared to the time interval of charge generation, the peak voltage $|\Delta U|$ can be evaluated to obtain the number of generated electrons $N_e$ by the following expression:

$$N_e = C_p \Delta U / e, \tag{1}$$

where $C_P$ is the gap capacitance and $e$ is the electron charge.

To investigate the validity of Eq. (1), we start with the *RC* response time of the measuring circuit, which was found to be approximately 1 ms from the experimental values for $R$ and $C_P$. The charge drift time constants and the charge drift velocities (for both electrons and ions) for the fields applied here (from 0.1 to 1 kV cm$^{-1}$ bar$^{-1}$ in He, Ne, and Ar) were obtained from Refs. 16–18. We obtained an almost gas independent electron drift velocity between $10^5$ cm s$^{-1}$ (for a weak field of 0.1 kV cm$^{-1}$ bar$^{-1}$) and $10^6$ cm s$^{-1}$ (for a strong field of 1 kV cm$^{-1}$ bar$^{-1}$). As the ion drift velocities are usually measured in somewhat stronger fields, we have extrapolated the data from Ref. 19, which were obtained over the range of 1–10 kV cm$^{-1}$ bar$^{-1}$. The extrapolation yields drift velocities over the range of $10^3$ to $10^4$ cm s$^{-1}$, where the lower value corresponds to lower fields and the heavier Ar ions. With these velocities and the typical gap length of 1 cm in our experiments, we find a drift time for electrons of the order of 1–10 $\mu$s, while the drift time for ions is roughly a thousand times longer, ranging from 0.1 to 1 ms. With these values showing that the electron drift time is much smaller than the other time constants, Eq. (1) is a good approximation to determine the number of generated electrons.

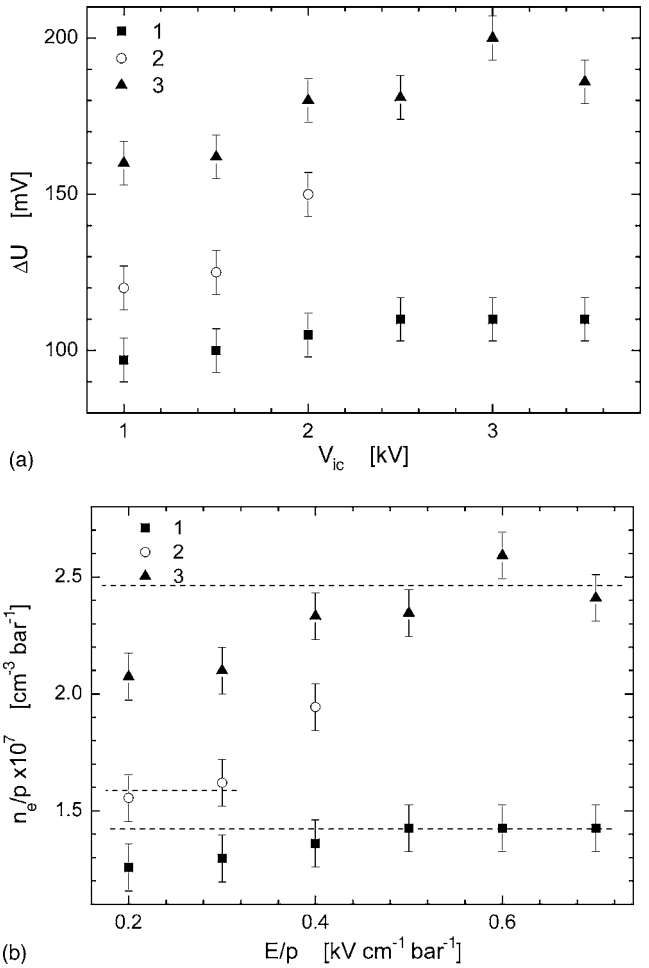


FIG. 3. (a) Discharge voltage change $\Delta U$ measured as function of the drift voltage $V_{IC}$. (b) The same data are plotted as the specific electron density $n_e/p$ vs the specific electric field $E/p$. The gases used are He [Eq. (1)], Ne [Eq. (2)], and Ar [Eq. (3)] at $p=5$ bar, with $d=1$ cm. The horizontal lines correspond to the specific preionization density.

From general considerations, the response of an *RC*-circuit to a very short signal ($\tau \ll RC$) is proportional to the integral of the signal and it shows an exponential growth. This is definitely the case for the electrons in our experiments. The ion drift time is comparable to the *RC* response time, thus the response of the *RC*-circuit to the ion current is more complicated. It is given by a convolution of the ion current waveform with an exponential *RC* response that is easily derived analytically. We developed a numerical simulation using the analytical derived convolution, experimentally relevant electron and ion drift times and a triangular

shape of the electron, and ion current, as proposed in Ref. 6. The calculated response is very similar to the experimentally observed signal amplitude, timing, and shape (excluding the noise related sharp spike). This argument holds over a wide range of electron and ion velocities. The amplitude of the calculated signal differs from the expected *RC*-response to the electron charge [as given by Eq. (1)] by less than 10% in all cases.

For better comparison between the experimentally obtained results with the theoretically expected values (see Secs. IV and V), it is convenient to determine the absolute number of electron $N_e$ from either the electron density $n_e = N_e/V$ or the specific electron density $n_e/p$. Here, $V$ is the gas volume irradiated by x rays which, in our setup, is well defined by the various apertures and windows as $V=Sd$, where $S$ is the area of the (1 cm diameter) input window, flange opening, and lead aperture. The measured specific electron density can then be obtained from experimental data as

$$\frac{n_e}{p} = \frac{C_p \Delta U}{pedS}, \tag{2}$$

provided that the drift field is large enough to collect all the generated electrons, and that the field is small enough not to generate excess charge by initiating electron avalanches. To ensure that ionization measurements were performed with the appropriate drift field, we measured $\Delta U$ as a function of the applied drift voltage $V_{IC}$, as is shown in Fig. 3(a). To obtain a gas-specific ionization measure, which is independent of the particular pressures and gap lengths used, we replotted the data in Fig. 3(b). $\Delta U$ transformed into the specific electron density and $V_{IC}$ transformed into the specific electric (drift) field defined as [using Eq. (2)]

$$\frac{E}{p} = \frac{V_{IC}}{pd} \tag{3}$$

For He [Eq. (1)] and Ar [Eq. (3)], it can be seen that $\Delta U$ and $n_e/p$ initially increases with $V_{IC}$, and thus, with the specific electric field also before $n_e/p$ saturates. The saturation value, as indicated by the horizontal dashed lines, is called the specific preionization electron density, where all the generated charge is collected and no excess charge is generated.

For Ne [Eq. (2)] it can be seen that $\Delta U$ ($n_e/p$) increases only slightly between $V_{IC}=1$ and 1.5 kV ($E/p$ between 0.2 and 0.3 kV cm$^{-1}$ bar$^{-1}$), but there is a strong increase between 1.5 and 2 kV (0.2 and 0.4 kV cm$^{-1}$ bar$^{-1}$). Beyond 2 kV, we found electric gas breakdown. From this we conclude that the generated charge at 2 kV includes some excess charge already. Consequently the value of the specific preionization electron density of He is found between 1 and 1.5 kV, where the charge variation with the drift voltage is smallest.

In our experiments, the saturation voltage is typically ~1–2 kV, which corresponds to a specific electric field strength of ~0.2–0.4 kV cm$^{-1}$ bar$^{-1}$ or ~0.8–1.6 Td. The saturation voltage allows the space charge region to fill the whole electrode gap and is given by[4]

$$V_{\min} = \frac{end^2}{2\varepsilon_0}, \tag{4}$$

where $e$ is the elementary charge and $\varepsilon_0$ is the permittivity of vacuum. After substituting $d=1$ cm and $n=10^8$ cm$^{-3}$, which are typical values in our experiments, we calculate that $V_{\min}$ is ~100 V, which is ten times lower than the experimentally observed saturation voltage. On the other hand, Eq. (4) gives the minimum required voltage necessary to pull all electrons from the bulk over an infinite time. Our measurements are based on Eq. (1), which is valid only when the electron drift time is much shorter than the *RC* time of the measuring system which is itself much shorter than the ion drift time. Therefore, in our experiments, the electric field has to be stronger than Eq. (4) suggests. But it has to be weak enough to avoid additional ionization in the volume due to accelerated electrons. As long as additional ionization is negligible, an increase of the applied voltage does not change the electron and ion concentration in the bulk, but affects the convoluted *RC* response of the measuring system. If the electron drift time is larger or comparable to the *RC* time of the circuit, the amplitude of the signal is not proportional to the electron density. The integral of the signal should be taken as a measure for the electron density instead. On the contrary, for stronger electric fields, when the *RC* time is shorter than the electron drift time, Eq. (1) is valid. This explains the small changes in the amplitude of the signal with the applied voltage in Fig. 3(a), while the applied voltage is ten times higher than $V_{\min}$ given by Eq. (4) already.

From Refs. 20–22 we can conclude that in He and Ar gases, electron impact ionization is negligible in an electric field of ~1 Td, while in Ne it may affect the measurements. For Ne the electric field is too strong, so that additional volume ionization takes place and the ionization density increases steeply with the electric field,[20–22] as can be seen in Fig. 3(a) [Eq. (2)]. Thus, the electron density in Ne may be overestimated. Therefore the experimental determination of the saturation voltage gives more adequate results than calculated values from Eq. (4).

With the described procedure, we found the following specific preionization electron densities: $1.4 \times 10^7$ cm$^{-3}$ bar$^{-1}$ for He, $1.6 \times 10^7$ cm$^{-3}$ bar$^{-1}$ for Ne, $2.5 \times 10^7$ cm$^{-3}$ bar$^{-1}$ for Ar, $2.2 \times 10^7$ cm$^{-3}$ bar$^{-1}$ for a 99:1 He:Xe mixture, and $1.6 \times 10^7$ cm$^{-3}$ bar$^{-1}$ for a 99.9:0.1 He:$F_2$-mixture, all obtained at a total gas pressure of 5 bars and a gap length of 1 cm. It can be seen that the preionization densities achieved in different gases do not differ from each other much. For example, the $N_e$ measured in Ar [Eq. (3)] is only about two times higher than in He [Eq. (1)], although Ar absorbs x rays more effectively than He, an observation which will be discussed below (Secs. IV and V).

Measurements of $N_e$ and $n_e/p$ versus the gap length (in the saturated regime, as described in Fig. 3) are shown in Figs. 4(a) and 4(b), respectively. The measurements were performed with He [Eq. (1)], Ne [Eq. (2)], and Ar [Eq. (3)] at $p=5$ bars. It can be seen that, within the experimental errors that arise from the uncertainty in the drawing of the saturation lines in Fig. 3(b), there is no strong dependence on the gap length $d$. Particularly, in Fig. 4(a), $N_e$ does not grow in

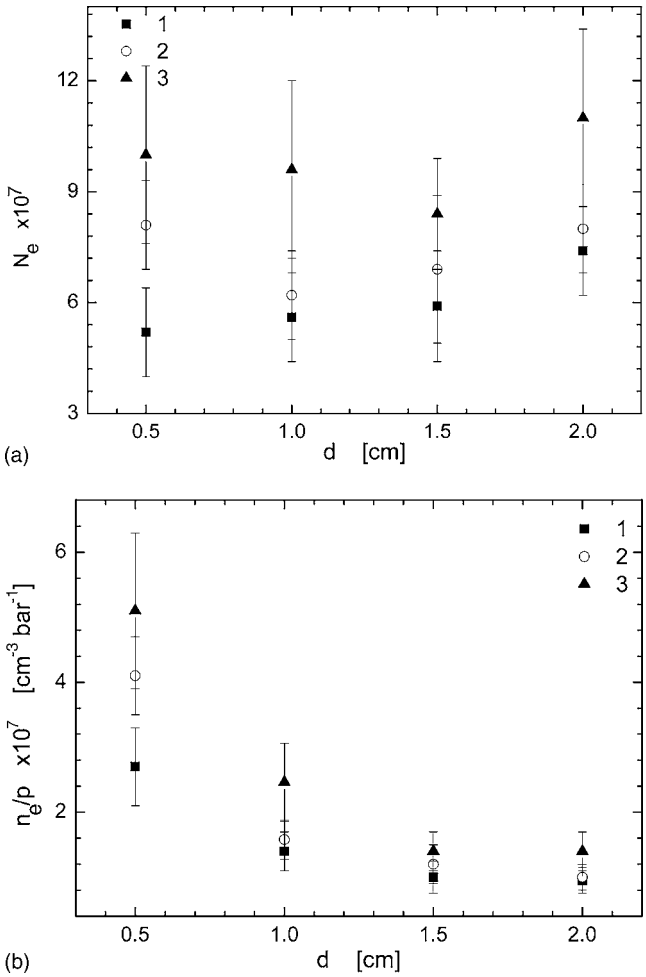


FIG. 4. Saturated total number of the electrons gathered (a) and the saturated specific electron density (b) measured vs the gap length of the ionization chamber in He [Eq. (1)], Ne [Eq. (2)], and Ar [Eq. (3)] at $p=5$ bars.

proportion with $d$, although this would be expected according to the standard picture of x-ray preionization, as shown in Sec. IV. Instead, $N_e$ seems to have some weak minimum for Ne [Eq. (2)] and Ar [Eq. (3)], and $N_e$ grows only slightly with $d$ in He [Eq. (1)]. When transformed to specific densities [Fig. 4(b)], the absence of growth of $N_e$ with $d$ for Ne and Ar shows a drop of $n_e/p$ versus $d$, which is almost inversely proportional to $d$.

Additional measurements were carried out with He at gas pressures from 1 to 5 bars with a constant gap length of 1.5 cm. The results, including those from Fig. 4, are summarized in Fig. 5, which shows $N_e$ (solid squares) and $n_e/p$ (open circles) measured versus the specific gap length, $p \times d$. One sees some growth of $N_e$ with $p \times d$, although well below proportionality and, correspondingly, one sees a decrease of $n_e/p$ with increasing $p \times d$, although not as strong as proportional to $1/(pd)$.

To summarize the experimental observations, for He, Ne, and Ar, we have obtained specific ionization densities of 1.4, 1.6, and $2.5 \times 10^7$ cm$^{-3}$ bar$^{-1}$. This should be compared with what is theoretically expected from x-ray absorption in these gases, i.e., if one wants to address the observed ionization to absorption of x rays in the gas volume. The other observation is that the total number of electrons does not

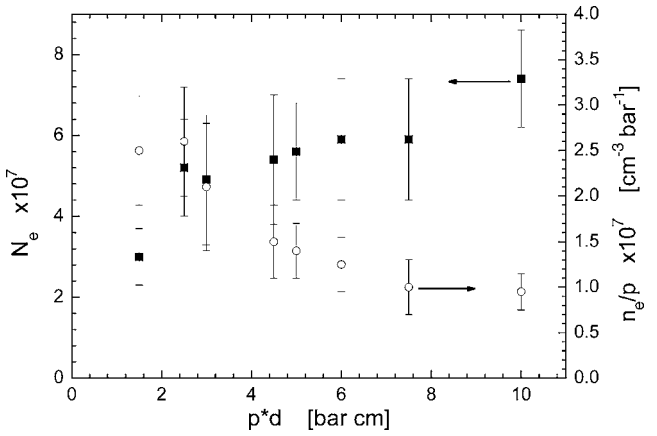


FIG. 5. Saturated total number of electrons collected (solid squares, left axis) and the saturated specific electron density (open circles, right axis) measured vs the specific length $pd$ of the gap of the ionization chamber, measured in He.

grow in proportion with the gap length for Ne and Ar, and that it grows only slowly with the gap length for He. When expressed as the specific preionization density this corresponds to a near-$1/d$ decrease of $n_e/p$ for Ar and Ne, and for He it corresponds to some weaker decrease of $n_e/p$ with $p \times d$. These observations need to be compared with the assumption that the preionization is based on the absorption of x rays in the gas volume as well.

## IV. ELECTRON DENSITIES EXPECTED FROM X-RAY ABSORPTION IN GAS

To draw conclusions on the underlying ionization mechanism, we calculate the theoretically expected electron densities for comparison with the experimental data. We assume for now that the ionization is solely caused by the absorption of x rays in the various gases and start with a general check on the overall number of electrons observed.

To indicate why it is worthwile to do this estimate in more detail, we start by showing how even a very basic calculation deviates from what is expected. The measured x-ray dose of 1 mrad/pulse in the discharge chamber corresponds to an absorbed energy-mass ratio of $6.25 \times 10^{13}$ eV/kg, which with a typical ionization energy for atoms of the order of 10–100 eV, should generate $10^{12}$–$10^{13}$ electrons/kg of irradiated gas. The masses of the irradiated gases at 5 bars in the discharge chamber are $6.64 \times 10^{-7}$ kg (He), $3.36 \times 10^{-6}$ kg (Ne), and $6.64 \times 10^{-6}$ kg (Ar) as can be calculated from their specific weight (He: $1.66 \times 10^{-4}$ g/cm$^3$, Ne: $8.39 \times 10^{-4}$ g/cm$^3$, Ne: $1.66 \times 10^{-3}$ g/cm$^3$ at 1 bars)[23,24] and from $V=S \times d=0.8$ cm$^3$. Thus from the dose applied we expect approximately $10^{12}$–$10^{13}$ electrons/kg. From the data in Fig. 4(a) it can be obtained that the measured numbers are 8, 1.8, and $1.5 \times 10^{13}$ electrons/kg in He, Ne, and Ar, respectively, and thus consistent with the prediction.

In Ref. 25 it is reported that due to the housing of the SEQ-6 pen dosimeter, which simulates the x-ray absorption of the soft tissues of the human derma, the dose measured by this pen dosimeter is two times lower than the dose measured by a LiF thermoluminescent detector. As this correction fac-

TABLE I. The $(\mu_E/\rho)_G\ \rho_G$ [cm$^{-1}$] values relevant for the absorption of x rays in different gases at a pressure of 5 bars vs the x-ray photon energy.

| | 30 keV | 56 keV | 100 keV |
|---|---|---|---|
| He | $7.8\times10^{-6}$ | $1.1\times10^{-5}$ | $1.7\times10^{-5}$ |
| Ne | $1.5\times10^{-3}$ | $4.7\times10^{-4}$ | $1.2\times10^{-4}$ |
| Ar | $2.2\times10^{-2}$ | $3.1\times10^{-3}$ | $6.0\times10^{-4}$ |

TABLE II. The $(\mu_E/\rho)/A_I$ [cm$^2$ g$^{-1}$ eV$^{-1}$] values for different gases and x-ray photon energies.

| | 30 keV | 56 keV | 100 keV |
|---|---|---|---|
| He | $2.2\times10^{-4}$ | $3.0\times10^{-4}$ | $4.7\times10^{-4}$ |
| Ne | $1.0\times10^{-2}$ | $3.1\times10^{-3}$ | $7.8\times10^{-4}$ |
| Ar | $1.0\times10^{-1}$ | $1.4\times10^{-2}$ | $2.8\times10^{-3}$ |

tor depends on the x-ray spectrum, which may differ in our setup from Ref. 25, it is omitted from our estimations.

However, there remains a striking inconsistency, as was pointed out above. The absorption of x rays increases strongly with the atomic mass such that one would expect a much higher electron number in Ar compared to He, while the experimental data show the opposite trend.

To better quantify the latter expectation we start by calculating what amount of x-ray energy is absorbed in the various gases, $\Delta W$, via Lambert–Beer's law assuming weak absorption,

$$\Delta W = W_0 - W(x) \approx W\left(\frac{\mu_E}{\rho}\right)_G \rho_G x. \tag{5}$$

Here, $W_0$ is the energy of an incident x-ray pulse, $W(x)$ is the intensity remaining after absorption, $(\mu_E/\rho)_G$ is the gas-type-specific absorption coefficient, $\rho_G$ is the density of the gas which is proportional to the gas pressure $p$, and $x$ is the absorption path length. In the experiments the path length is equal to the electrode gap $(x=d)$. The assumption of weak absorption is well justified (see below).

Equation (5) is valid for monochromatic x-ray radiation, whereas our source emits a broad spectrum. To take this into account, we discuss the spectrum of x rays arriving in the ionization chamber, by taking into account the spectrum of the source, and the filtering of the radiation on its way into the chamber. Our source is a typical x-ray emitter with its spectrum given by the acceleration voltage (100 kV) and the high-$Z$ target material. In our case, the characteristic radiation mostly comes from a $K\alpha$ line with a photon energy of $\sim$56 keV, and there is a continuous Bremsstrahlung spectrum that decreases toward the high-energy cutoff at 100 keV. To consider how the spectrum is modified by traveling into the discharge chamber, we recall that the radiation travels through 2 mm of Al, which is the total thickness of the source output window plus the discharge chamber input window. Using known x-ray absorption data of Al, one finds that about 25% of the 10 keV photons, 81% of the 20 keV photons, and 94% of the 30 keV photons are transmitted into the chamber.[23,24] Photons with lower energy ($<$5 keV) are almost entirely absorbed, while photons with energy higher than 50 keV are almost fully transmitted. Based on these numbers, and to simplify the discussion, we have restricted ourselves considering three representative spectral ranges where a significant x-ray flux is expected in the discharge chamber, namely, 30, 56, and 100 keV.

To illustrate the typical relative strength of the x-ray absorption at these energies for He, Ne, and Ar at 5 bar pressure, we have summarized in Table I the $(\mu_E/\rho)_G\rho_G$ value which governs the absorbed energy in Eq. (5).[23,24] Corresponding calculations for the mixtures of light and heavy gases (e.g., 99.9% He with 0.1% Xe) are omitted here for brevity.

It can be seen that the absorption is indeed weak $[(\mu_E/\rho)_G\rho_G d \ll 1]$ for all gap lengths, gases, photon energies, and pressures used in our experiment, thus validating Eq. (4). Furthermore, it can be seen that the x-ray absorption in Ar is large compared to He. For example, Ar absorbs 30 keV photons about 2800 times more efficient and 100 keV photons 35 times more efficient than He. These ratios are still high, $\approx$190 and 7, respectively, when comparing Ne with He.

The next step is to estimate the relative number of generated electrons for comparison with Figs. 4(a) and 5. For this we take into account that the absorption of an x-ray photon generates a primary photoelectron with almost the same energy and that, subsequently, secondary electrons are generated. The average energies to generate an electron-ion pair in this process are $A_I$=43 eV for He, 36 eV for Ne, and 26 eV for Ar,[23,24] such that the total number of generated electrons is given by

$$N_e = \Delta W/A_I = W_0\left(\frac{\mu_E}{\rho}\right)_G \frac{\rho_G^0}{p^0 A_I} pd. \tag{6}$$

Here, for an easier discussion of pressure dependencies we have expressed the gas density $\rho_G$ in Eq. (5) via the gas pressure $p$, using $\rho_G = p\times\rho_G^0/p^0$, where $\rho_G^0$ is the mass density at standard pressure, $p^0$=1 bar. Equation (6) predicts that $N_e$ grows proportionally with the pressure $p$ and the gap length $d$.

Finally, from dividing Eq. (6) by the absorbing volume $V=S\times d$ and the pressure $p$, one obtains the specific preionization density to compare with the experimental data in Figs. 4(b) and 5,

$$n_e/p = N_e/(Vp) = W_0\left(\frac{\mu_E}{\rho}\right)_G \frac{\rho_G^0}{p^0 A_I S}. \tag{7}$$

Equation (7) shows the advantage of defining the specific ionization density. There is no dependence on $d$ and $p$, and as the other parameters in Eq. (7) are held constant in the experiments (such as $W_0$ and $S$), $n_e/p$ should only depend on the type of gas used, via the factor $(\mu_E/\rho)_G/A_I$. To show the predicted dependence for the gases used, this factor is given in Table II for the three photon energies considered.

One can see that the specific electron density should be about 450 times higher in Ar, and 45 times higher in Ne than in He at 30 keV, and the corresponding ratios should be 45 and 10 (at 56 keV) and 6 and 1.7 (at 100 keV). This is, however, in clear contradiction with the experimental data, where we found a much smaller ratio of about 2 for (Ar versus He) and of 1.1 (Ne versus He).

There is a second contradiction, namely, that the data in Table I and thus the expected $N_e$ in Eq. (6), should increase proportionally with both $p$ and $d$ [see Eq. (6)]. Such an increase is, however, not seen in the experimental data, where $N_e$ shows only a weak variation with $d$ [Fig. 4(a)]. Another way to state this is that the data in Table II, and thus, $n_e/p$ in Eq. (7), are independent of $d$, while the experimental data [Fig. 4(b)] shows a strong decrease with $d$. The only gas where the experimental data somewhat resemble the prediction is He. Indeed, Fig. 4(a) shows some weak growth of $N_e$ with $d$ (where a strong proportional growth is predicted), and in Fig. 4(b) $n_e/p$ shows some weak decrease versus $d$ (where a constant value is expected). Similarly, as seen in Fig. 5, He shows a small growth of $N_e$ with $p \times d$ (where a proportional growth is expected), and it shows a weak decrease of $n_e$ with $p \times d$ (where a constant value is expected).

In summary, we conclude from these contradictions that the generated electron densities do not arise only from the absorption of x rays in the gas. This means that a different mechanism is responsible for the observed ionization. It is thus important to identify this mechanism because its properties may be relevant for optimizing the beam quality of excimer lasers.

## V. PHOTOELECTRIC EFFECT AT THE CATHODE

The observed phenomena can be explained if the photoelectric effect at the cathode is taken into account. When an x-ray photon is absorbed in the cathode, a metal atom is ionized and a free electron is released. If the ionization takes place from an outer shell, this produces a fast electron with energy comparable to the photon energy. However, as the x rays traverse the cathode, most of these primary photoelectrons are produced in the bulk of the cathode and, subsequently, they experience a strong slowing down by inelastic collisions. As a result, most primary electrons from the bulk, and also secondary electrons created in the bulk, do not enter the gas volume in the chamber because, when they arrive at the cathode surface, their energy is not sufficient to overcome the work function barrier.

However, a small fraction of the x-ray photons are absorbed inside a thin boundary layer just under the cathode surface and thus primary electrons are generated in close proximity to the surface. When electron generation occurs at a distance which is comparable to or smaller than the mean escape depth (MED) these primary electrons can enter the gas volume without significant energy loss. In the gas they may ionize atoms and generate a large number of secondary electrons, when the primary electron energy is much larger than the average energy required for secondary ionization. We will show in the following that, depending on the parameters involved, the electron density generated by such cathode photoelectrons may be much larger than that from direct absorption of x rays in the gas.

A first step in calculating the strength of ionization by cathode photoelectrons is to estimate the MED in our setup. Corresponding calculations are well known from Auger electron spectroscopy and x-ray photoelectron spectroscopy. There, however, relatively low photon energies are used (in the order of the ionization potential) such that the MED is usually comparable to the inelastic mean free path (IMFP) $\lambda_I$.[26] In our case of much higher photon energies, the electrons can still enter the gas volume with tens of keV energy, even when loosing a significant part of their initial kinetic energy when generation occurred deeper in the cathode. Thus, we expect that the MED in our case is longer than the IMFP and, instead, comparable to a range $R$, after which high-energy electrons come to a full stop in the electrode material.

To determine $R$, we performed calculations in the continuous slowing-down approximation (CSDA), starting with an initial kinetic energy in the 50–60 keV region. In Ni, of which the 30 $\mu$m thick cathode top layer is made, we obtain a range of $R=9$ $\mu$m.[27] As a conservative measure for the MED in our case, which we call $d_{es}$, we decided to choose a value of $d_{es}=R/2=4.5$ $\mu$m because then the escaping electrons still possess most of their initial energy, about 75%. In the second step, we use the obtained MED in Lambert–Beer's law to determine the x-ray energy absorbed in the relevant Ni top layer of the cathode, i.e., within $d_{es}=4.5$ $\mu$m. The energy absorbed is then transported as fast primary photoelectrons into the gas volume and can, thus, be compared with the energy that would be deposited directly in the gas volume by direct x-ray absorption.

We determine the x-ray energy $\Delta W_{Ni}$ absorbed in the Ni escape layer (thickness $d_{es}$) as

$$\Delta W_{Ni} = W_0 \left( \frac{\mu_E}{\rho} \right)_{Ni} \rho_{Ni} d_{es} \approx W_0 8 \times 10^{-3}, \tag{8}$$

for which we have used the mass attenuation coefficient of Ni for 50–60 keV photons, $(\mu_E/\rho)_{Ni}$, and the mass density of Ni, $\rho_{Ni}$. It can be seen that the thin Ni layer does not noticeably reduce the x-ray energy transmitted into the gas, however, about 75% of the absorbed energy $\Delta W_{Ni}$ arrives in the gas volume as primary photoelectrons, which is approximately $6 \times 10^{-3} W_0$. Of course, the generated photoelectrons are locally emitted over the $4\pi$ full solid angle and less than one-half of them can escape into the gas volume. Compared to the arbitrary choice of the MED in our order-of-magnitude calculations this geometry coefficient is not important.

This value is to be compared with the x-ray energy that is directly absorbed in the gas, $\Delta W_G$, which is given by (see Sec. IV),

$$\Delta W_G = W_0 \left( \frac{\mu_E}{\rho} \right)_G \rho_G d. \tag{9}$$

By using the data from Table I at 56 keV and taking $d=1$ cm, the typical gap length used in the experiments, we find a directly absorbed energy of $\Delta W_G = 1.1 \times 10^{-5} W_0$ for He, $\Delta W_G = 4.7 \times 10^{-4} W_0$ for Ne, and $\Delta W_G = 3.1 \times 10^{-3} W_0$ for Ar.

From the latter numbers it can be seen that photoemission from the cathode can easily dominate the energy of direct x-ray absorption in the gas. In our estimate, photoemission dominates by almost a factor of 10 in He, by a factor of 5 in Ne, and even in Ar more than 50% of the ionization should come from the photocathode.

TABLE III. The range $L_C$ of cathode photoelectrons [cm] values for different gases at $p=5$ bars and different initial kinetic energies.

| | 30 keV | 56 keV | 100 keV |
|---|---|---|---|
| He | 2.1 | 6.2 | 18 |
| Ne | 0.52 | 1.5 | 4.2 |
| Ar | 0.31 | 0.89 | 2.4 |

Besides these numbers, there are typical signatures to be expected, provided that the primary cathode electrons come to a full stop after a characteristic length $L_C$ shorter than the gap length $d$: the number of electrons should be independent of the gas pressure and the gap length. Only a dependence on the type of gas should remain because the number of secondary electrons in the gas depends on the average energy loss in an ionization act, which is somewhat larger for a gas with a higher atomic weight. To summarize, when the gap length is larger than the characteristic propagation length of electrons, the total number of electrons should be independent of the gap length, such that the specific electron density drops as $1/d$. Simultaneously, there should be a slightly stronger ionization for heavier gases. Note that this is indeed observed in Fig. 4. From this we conclude that the observed ionization densities are caused by x-ray-induced photoemission from the cathode.

## VI. INFLUENCE OF CATHODE PHOTOELECTRON RANGE ON THE PREIONIZATION DENSITY

The signature of cathode photoelectron-based ionization can be identified as a clear $1/d$ dependence of $n_e/p$, if the characteristic propagation length $L_C$ of fast cathode electrons is shorter than the gap length $d$. Otherwise these electrons would not loose all of their energy via ionization of the gas and $N_e$ would then grow with $d$, weakening the $1/d$-decay of $n_e/p$. To see whether $L_C$ is smaller than $d$, we have calculated $L_C$ in He, Ne, and Ar,[27] for the three photoelectron energies of interest, using the CSDA.

The results of the calculations are presented in Table III for a pressure of $p=5$ bars, which is typical for high-power excimer lasers. It can be seen that results show a systematic decrease of $L_C$ toward lower kinetic energy. For a general interpretation of this, we note that, although excited by the same x-ray spectrum, cathode photoelectrons possess a lower average kinetic energy than primary photoelectrons from the gas due to collisional slowing in the cathode. As a result, cathode electrons should generally show a smaller $L_C$, and thus be more effective in transfering their kinetic energy to secondary electrons in the gas.

When looking more closely at Table III, one can see that the $L_C$ of the slower part of cathode electrons (in He at 30 keV, Ne and Ar at 30 and 56 keV) is below or comparable to the largest gap size used in the experiments ($d=2$ cm). Only for the fast part of the electrons (He at 56 and 100 keV, Ne at 100 keV, and Ar at 100 keV) is $L_C$ larger or much larger than 2 cm.

Compared to the experimental data, this is consistent with the observation that the number of electrons $N_e$ produced in He grew somewhat with $d$ (Fig. 5) and that $n_e/p$ somewhat decreases with $d$, but that in He and Ar $N_e$ stayed almost constant and $n_e/p$ decreased with a near $1/d$-dependence (Fig. 4).

To summarize, in our experiments the direct absorption of x-ray photons with energies between 30 and 100 keV is rather ineffective for preionization of the gas volume for two reasons: the first is the weak absorption of such x-ray photons in gases and the second is the long range of the primary fast electrons generated in the gas. Compared to this, photoemission from the cathode was found to be much more important and even largely dominant in some cases. For example, in He ($p=5$ bars and $d=1$ cm) we have estimated that cathode electrons produce roughly 600 times higher preionization than the direct absorption of x-ray photons in the gas. Even for Ar, which shows a much stronger x-ray absorption and a much shorter $L_C$ for photoelectrons, the ionization by cathode electrons remains comparable with direct x-ray ionization, at least for x-ray energies of up to 50 keV.

## VII. CONCLUSION

We experimentally investigated the x-ray preionization of high-pressure gases as used in high-power excimer lasers. For this, x rays were generated by stopping electrons accelerated from a pulsed vacuum corona discharge and, after collimation, the x rays were injected through Al windows into a separate discharge (ionization) chamber. The chamber was filled with various gases at mostly 5 bar pressure, while various electrode gap lengths were used in the range from 0.5 to 2 cm. The degree of ionization was measured by monitoring the discharge current induced by the x-ray pulses inside the discharge chamber.

With a dose of about 1 mrad/pulse, we observed a specific preionization electron density of the order of $10^7$ cm$^{-3}$ bar$^{-1}$, rather independent of the gas used (He, Ne, and Ar), or the gas mixtures used (He with $F_2$, at a 99.9:0.1 ratio, and He with Xe at 99:1). We found that, at constant pressure, the specific electron density decreased with increasing gap length and our estimations show that this is in contradiction with the standard picture, where x-ray preionization in excimer lasers is understood as the result of direct absorption of x rays in the laser gas. Further, we found that preionization in the heaviest gas (Ar) is only two times higher than in the lightest gas (He) which is, again, in contradiction with the picture of direct x-ray absorption.

As the physical mechanism which is responsible for the experimental observations, based on estimates, we identified the generation of fast photoelectrons from the cathode, through which the x rays are usually injected. With the characteristic lengths used, $p\times d<10$ bar cm, we found that in He the cathode electrons strongly dominated the preionization. Even with heavy gases which show a much stronger x-ray absorption and primary electron deceleration, the cathode-based ionization remained comparable with direct x-ray ionization.

From this we concluded that the role of direct x-ray preionization is, so far, largely overestimated, and that the

role of the photoelectric effect in the cathode is largely underestimated, particularly in the medium size discharges ($p \times d < 10$ bar cm) as investigated here.

Only in large scale lasers, operating with $p \times d$ in excess of 100 bar cm, and only in the bulk of the discharge, the generation of a homogeneous preionization should be addressed to direct x-ray absorption. However, cathode-based ionization remains a significant contribution, or even strongly dominating, in a $p \times d \approx 1$ bar cm thick enhancement layer in front of the cathode, and the homogeneity of this higher-density layer may play a central role for the homogeneity of the main, laser-pumping discharge. This is because the electrons within this enhancement layer are accelerated and, thus, produce further electrons throughout the entire discharge gap, thereby possibly dominating the main discharge dynamics across its entire length. Although different mechanisms may contribute to the development of discharge instabilities; for example, local field enhancement on small imperfections of the cathode surface or a number of chemical reactions and physical processes such as stepwise ionization or photodetachment,[28] the necessity of homogeneous volume preionization for stable high-pressure gas discharges is evident. Finally, we note that the described cathode-based ionization effects may well be of relevance for adequate modeling of the filamentation of excimer laser discharges,[29–31] where the preionization density is a key parameter. Photoelectric cathode-based preionization might also be of relevance for recent observations[32] that the addition of Xe to $F_2$ based excimer discharges strongly improved the discharge homogeneity.

## ACKNOWLEDGMENTS

The authors appreciate the stimulating interest of Dr. S.V. Mitko during the course of these experiments. This research is supported by the Dutch Technology Foundation STW, Applied Science Division of NWO (the Netherlands), and the Technology Program of the Ministry of Economic Affairs of the Netherlands.

[1] A. J. Palmer, Appl. Phys. Lett. **25**, 138 (1974).
[2] J. I. Levatter, and Sh.-Ch. Lin, J. Appl. Phys. **51**, 210 (1980).
[3] H. M. J. Bastiaens, S. J. M. Peters, X. Renard, P. J. M. Peters, and W. J. Witteman, Appl. Phys. Lett. **72**, 2791 (1998).
[4] G. Giordano, T. Letardi, and C. E. Zheng, Nuovo Cimento Soc. Ital. Fis., B **101**, 561 (1988).
[5] R. J. M. Bonnie, J. W. Gerritsen, and R. S. Zuidema, J. Appl. Phys. **65**, 4521 (1989).
[6] F. A. van Goor, J. Phys. D **26**, 404 (1993).
[7] W. H. Bragg, *Studies in Radioactivity* (Mac Millan, London, 1912).
[8] L. H. Gray, Proc. R. Soc. London, Ser. A **122**, 647 (1929).
[9] L. H. Gray, Proc. R. Soc. London, Ser. A **156**, 578 (1936).
[10] G. W. C. Kaye and W. Binks, Proc. R. Soc. London, Ser. A **161**, 564 (1937).
[11] S. Humphries, J. J. Ramirez, and M. G. Wilde, IEEE Trans. Plasma Sci. **8**, 517 (1980).
[12] J. I. Levatter, R. L. Sandstrom, and J. H. Morris, Proceedings of the IEEE Fourth Pulsed Power Conference, 1983 (unpublished), p. 755.
[13] S. J. Scott, J. Appl. Phys. **64**, 537 (1988).
[14] S. J. Scott, Appl. Phys. B: Photophys. Laser Chem. **56**, 201 (1993).
[15] H. M. J. Bastiaens, Ph.D. thesis, University of Twente, 2000.
[16] R. A. Nielsen, Phys. Rev. **50**, 950 (1936).
[17] J. A. Hornbeck, Phys. Rev. **83**, 374 (1951).
[18] J. S. Townsend and V. A. Bailey, Philos. Mag. **46**, 657 (1923).
[19] J. A. Hornbeck, Phys. Rev. **84**, 615 (1951).
[20] A. V. Phelps and Z. Lj. Petrović, Plasma Sources Sci. Technol. **8**, R21 (1999).
[21] A. L. Ward, Phys. Rev. **112**, 1852 (1958).
[22] H. Brunet, B. Lacour, J. R. Serra, M. Legentil, S. Mizzi, S. Pasquiers, and V. Puech, J. Appl. Phys. **68**, 4474 (1990).
[23] J. H. Hubbell, Int. J. Appl. Radiat. Isot. **33**, 1269 (1982).
[24] S. M. Seltzer, Radiat. Res. **136**, 147 (1993).
[25] S. Bollanti, P. Di Lazzaro, F. Flora, G. Giordano, T. Letardi, G. Schina, and C. E. Zheng, Rev. Sci. Instrum. **65**, 315 (1994).
[26] A. Jablonski and I. S. Tilinin, Phys. Rev. B **54**, 10927 (1996).
[27] NIST database, ELSTAR, http://physics.nist.gov/PhysRefData/Star/Text/contents.html.
[28] M. R. Osborne, R. J. Winfield, and G. M. Green, J. Appl. Phys. **65**, 5242 (1989).
[29] D. Mathew, H. M. J. Bastiaens, K.-J. Boller, and P. J. M. Peters, Appl. Phys. Lett. **88**, 101502 (2006).
[30] D. Mathew, H. M. J. Bastiaens, K.-J. Boller, and P. J. M. Peters, Proc. SPIE **6346**, 63460Q (2006).
[31] D. Mathew, H. M. J. Bastiaens, K.-J. Boller, and P. J. M. Peters, J. Appl. Phys. **102**, 033305 (2007).
[32] D. Mathew, H. M. J. Bastiaens, K.-J. Boller, and P. J. M. Peters, Appl. Phys. B: Lasers Opt. (submitted).